

Surface-Rearranged Pd₃Au/C Nanocatalysts by Using CO-Induced Segregation for Formic Acid Oxidation Reactions

Sang-Young Lee,^{†,‡} Namgee Jung,[†] Jinwon Cho,[†] Hee-Young Park,[†] Jaeyune Ryu,[†] Injoon Jang,[†] Hyoung-Juhn Kim,[†] EunAe Cho,[†] Yeung-Ho Park,[‡] Hyung Chul Ham,[†] Jong Hyun Jang,^{*,†} and Sung Jong Yoo^{*,†}

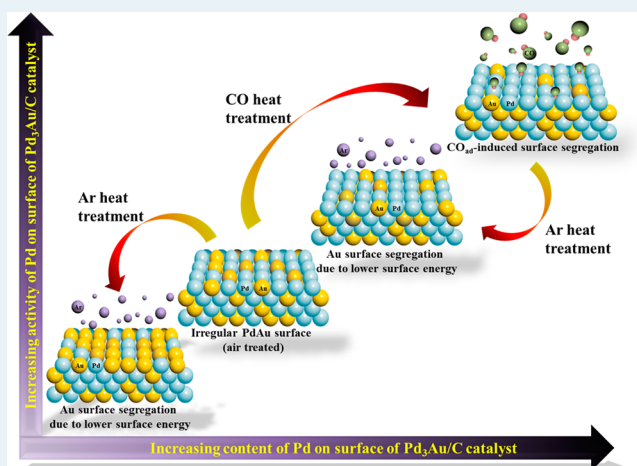
[†]Fuel Cell Research Center, Korea Institute of Science and Technology (KIST), Seoul 136-791, Korea

[‡]Department of Fusion Chemical Engineering, Hanyang University, Ansan 426-791, Korea

S Supporting Information

ABSTRACT: Carbon-supported Pd₃Au nanoparticle catalysts were synthesized via chemical reduction. Surface segregation of Pd in Pd₃Au catalyst was achieved via heat treatment under air, Ar, CO–Ar, and CO atmospheres, in order to obtain a surface with changed structures and composition. The surface composition was analyzed by electrochemical methods, and the Pd surface composition was observed to increase from 67.2% (air (asp) sample) to 80.6% (CO sample) after heat treatment under a CO atmosphere. The CO-induced surface segregation of the Pd₃Au electrocatalyst resulted in a significantly improved formic acid oxidation (from 6.93 to 18.11 mA cm⁻²) and stability (from 0.66 to 2.01 mA cm⁻²) compared to the sample prepared in air, as well as increased mass activity (from 199.20 to 520.55 A g⁻¹), electrochemical surface area (ESA_{Pd}) (from 61.08 to 95.68 m² g_{Pd}⁻¹), and specific activity (from 0.33 to 0.55 mA cm_{Pd}⁻¹), respectively. The electrochemical activities were significantly increased because of changes in the structure and composition of the surface due to the increased surface ratio of Pd promoted by CO heat treatment. The exchange of Pd and Au atoms between the surface and the bulk material was observed to influence formic acid oxidation and stable performance. The CO-induced surface segregation has the potential to greatly enhance the electrochemical activities and surface control of Pd–Au alloy nanoparticle with lower Pd contents.

KEYWORDS: formic acid oxidation, surface rearrange, Pd–Au alloy, nanocatalysts, CO-induced segregation



1. INTRODUCTION

The direct formic acid fuel cell is an attractive candidate for portable electronic devices applications because of the advantages of nontoxicity, nonflammability, and low-crossover effects through the Nafion membrane during the partial dissociation of formic acid.^{1–7} The oxidation of formic acid has been widely investigated as an electrochemical reaction in which the formic acid is oxidized to CO₂ through a dual pathway mechanism.⁸ The overall reactivity of the formic acid oxidation process by platinum-based catalysts is limited due to catalyst poisoning by CO (indirect pathway).⁹ In contrast, palladium-based catalysts have demonstrated excellent resistance to CO in such catalytic process,² and no adsorption of CO is observed during formic acid oxidation on Pd electrodes according to infrared reflection absorption spectroscopy (IRAS) studies (direct pathway).^{10,11}

In previous studies on the surface chemistry of such catalytic systems, the adsorption of CO on electrocatalyst surfaces was reported for various systems including single metal crystals,

core–shell materials, and various carbon-species-supported Pt- and Pd-based alloy catalysts through the scrutiny of their formic acid oxidation activity and IRAS.^{3,5,12–14} In particular, it was observed that the Pd metal and Pd-based alloy electrocatalysts proceeded via the direct pathway.¹⁵ Although Pd and Au are expensive materials, these are suitable for enhancement of formic acid oxidation activity. In addition, the Pd–Au electrocatalyst has been reported to enhance the overall performance of Pd due to the promoting effects of Au.¹⁶ The bulk composition of the various Pd–Au alloy electrocatalysts has been optimized for numerous applications depending on the Pd–Au ratios.⁴

The maximum formic acid oxidation rate depends on the Pd surface structure: Pd (100) > Pd (111) > Pd (110), as suggested by Hoshi et al.¹⁷ When the segregation energy (Pd–Au: 0.15

Received: February 20, 2014

Revised: June 9, 2014

Published: June 9, 2014

eV/atom) is positive, the hosted metal is expected to move into the bulk metal, thus forming new phases.¹⁸ We therefore intended to control the structure and Pd surface concentration without changing the bulk Pd–Au composition to facilitate the improvement of formic acid oxidation, characterizing the system by electrochemical methods; such methods are well-known tools to measure catalytic reactions at catalyst surfaces. In particular, the carbon monoxide adsorbed (CO_{ad}) oxidation is frequently used to measure the structure and composition of catalyst surfaces.^{19,20}

Nørskov et al. reported that using the properties of bimetallic alloys as a catalyst surface is a way of optimizing electronic structure.^{21–23} The one forming the strongest chemical bond with the adsorbates is expected with the more reactive alloy component segregating at the surface.^{24–28} In addition, we have previously reported that because of the simultaneous modification of both surface composition and electronic structure, CO-induced surface segregation is an attractive method to enhance electrocatalytic activity.^{29,30} The correlation between CO binding energy and surface segregation energy (surface free energy) of CO-induced segregation has been investigated by computational simulation for various metals and metal alloys.³¹ In this contribution, our aim was to further investigate the segregation of metal surfaces using a variety of atmospheric conditions and to assess the effect of such conditions on the nanoparticle size, surface structure, and ultimately, the catalytic behavior of such materials. We report the control of the Pd surface composition in Pd₃Au electrocatalysts accomplished by heat treatment under air, Ar, CO, and CO–Ar atmospheres. The bulk-scale electronic and compositional properties in Pd₃Au catalysts were measured by X-ray diffraction analysis and electrochemical techniques. The surface area ratio between Pd and Au at the Pd₃Au nanocatalyst surface was characterized by a combination of cyclic voltammetry (CV) and CO_{ad} oxidation. Through CO-induced surface segregation, the Pd surface structure and composition indicated promising levels of enhanced performance and stability toward formic acid oxidation.

2. EXPERIMENTAL SECTION

2.1. Materials. Palladium(II) acetylacetonate ($\text{Pd}(\text{C}_5\text{H}_7\text{O}_2)_2$, 99%), gold(III) chloride trihydrate ($\text{HAuCl}_4 \cdot 3\text{H}_2\text{O}$, $\geq 99.9\%$), oleylamine ($\text{C}_{18}\text{H}_{35}\text{NH}_2$, 70%), anhydrous ethanol ($\geq 99.5\%$), and borane *tert*-butylamine ($(\text{CH}_3)_3\text{CNH}_2 \cdot \text{BH}_3$) were purchased from Aldrich and used as received.

2.2. Synthesis. The carbon-supported Pd₃Au nanoparticle electrocatalysts (20 wt % metal, 3:1 molar ratio of Pd:Au) were prepared via borane *tert*-butylamine reduction in anhydrous ethanol at 30 °C. Carbon black (Vulcan XC-72, 0.1 g) was dispersed in anhydrous ethanol (100 mL); oleylamine (3.039 mmol) was then added to the dispersion with vigorous stirring and sonicated for 1 h. Palladium(II) acetylacetonate (0.145 mmol), gold(III) chloride trihydrate (0.048 mmol), and borane *tert*-butylamine (1.937 mmol) were dissolved in anhydrous ethanol (80, 20, and 20 mL, respectively). The metal precursors and reducing agent were quickly added in the order Au, Pd, and borane *tert*-butylamine to the dispersed carbon black solution at intervals of 30 min. The mixture was vigorously stirred for 24 h. After 24 h, this solution was filtered, washed, and dried. The heat treatment procedure involved heating the mixture from room temperature to 200 °C (at a rate of 10 °C/min), maintaining the material for 1 h at high temperature, before allowing it to cool to room temperature. To remove the

oleylamine surfactant on the catalyst surface, after drying in a vacuum oven overnight, all samples were subjected to heat treatment in air for 1 h at 200 °C in a tube furnace (only air-treated: asp). To achieve the enrichment of the Au or Pd at surface, the air-treated samples were heated under Ar or CO for 1 h at 200 °C (Ar or CO). The air–CO sample was heated under Ar at 200 °C for the reverse surface segregation (CO–Ar).

2.3. Catalyst Characterization. The molar ratio of catalyst was measured on an inductively coupled plasma (ICP-OES) spectrometer (Thermo iCAP 6300 series). Transmission electron microscopy (TEM) images (Philips CM30) were used to confirm the size and distribution of the Pd₃Au nanoparticles. X-ray diffraction patterns (XRD) were measured on a Rigaku D/MAX 2500 diffractometer equipped with a Cu $K\alpha$ X-ray source ($\lambda = 1.5401 \text{ \AA}$). X-ray photoelectron spectroscopy (XPS) of Pd 3d and Au 4f electrons was performed using a PHI-5000 Versa Probe (Ulvac-PHI). The binding energies of XPS experiments were calibrated by using a C 1s value of 284.6 eV. The fitting of XPS peaks was conducted using the XPSPEAK (version 4.1) program. XAS is measured at Pohang accelerator laboratory (PAL) with a ring current 200 mA at 3 GeV using the 10 C beamline. The fitting of XAS data was conducted using the Athena (0.8.056 version) program.

2.4. Electrochemical Measurements. Electrochemical analysis (Auto lab 302N potentiostat) of the catalysts was carried out using standard three-electrode electrochemical cell composed of a glassy carbon (GC) rotating disk electrode (5 mm diameter), Pt wire, and a saturated calomel electrode as the working, counter and reference electrodes, respectively. The appropriate ratio of catalyst ink components was prepared by mixing 10 mg of catalyst, 5 wt % Nafion solution (0.1 mL, Aldrich), and 2-propanol (1 mL). All potentials were measured with reference electrode without conversion. The electrochemical cell for cyclic voltammetry (CV) measurements was filled with 0.1 M HClO_4 (perchloric acid, ACS reagent, 70%, Aldrich) and purged with Ar for 30 min before use. Before the actual CV measurement, a potential range from -0.2 to 0.2 V was carried out to obtain the stable features of the experiment. The actual CV range from -0.2 to 1.2 V was performed with a scan rate of 20 mV/s to gain the Au surface area of catalyst for the Au reduction peak at ca. 0.8 V with a charge density of $400 \mu\text{C cm}^{-2}$.^{32,33} CO_{ad} oxidation was introduced for 10 min at -0.2 V . After CO_{ad} on the Pd₃Au nanoparticle surface, the electrochemical cell was saturated with an Ar atmosphere for 20 min. CO_{ad} oxidation measurements with a scan rate of 20 mV/s were conducted from -0.2 to 0.9 V with a charge density of $490 \mu\text{C cm}^{-2}$.³⁴ Formic acid oxidation measurements were performed from -0.2 to 1 V with a scan rate of 20 mV/s under an Ar atmosphere in $0.1 \text{ M HClO}_4 + 0.1 \text{ M HCOOH}$ solution (ACS reagent, 98–100%, Merck). Chronoamperometry (CA) was performed by holding the system at 0.1 V while measuring for 1 h under an Ar atmosphere in $0.1 \text{ M HClO}_4 + 0.1 \text{ M HCOOH}$ solution.

2.5. DFT Calculation. The calculations were performed on the basis of spin-polarized density functional theory (DFT) within the generalized gradient approximation (GGA-PW91),³⁵ as implemented in the Vienna Ab-initio Simulation Package (VASP).³⁶ The projector augmented wave (PAW) method with a planewave basis set was employed to describe the interaction between core and valence electrons.³⁷ An energy cutoff of 350 eV was applied for the planewave expansion of the electronic eigenfunctions. For the Brillouin zone integration, a $(2 \times 2 \times 1)$

Monkhorst–Pack mesh of k points was used to calculate geometries and total energies. For Pd₃Au (111) surfaces, a five atomic-layer slab was constructed with a hexagonal 4×4 unit cell. The slab was separated from its periodic images in the vertical direction by a vacuum space corresponding to seven atomic layers. The lattice constant for bulk Pd₃Au was predicted to be 4.03 Å, which is larger than the calculated bulk Pd lattice constant (3.96 Å). While the bottom two layers of the five-layer slab were fixed at corresponding bulk positions, the upper two layers were fully relaxed using the conjugate gradient method until residual forces on all the constituent atoms become smaller than 5×10^{-2} eV/Å.

3. RESULTS AND DISCUSSION

3.1. Characterization of the Pd₃Au Nanoparticles. With the synthesized nanoparticles in hand, we began a thorough investigation into their physical properties. The average molar ratio of the synthesized Pd₃Au catalysts was determined to be 2.9:1 as measured by ICP-OES. The schematic representing the surface segregation under Ar or CO atmospheres is shown in Figure 1. The enrichment of the Pd surface was accomplished

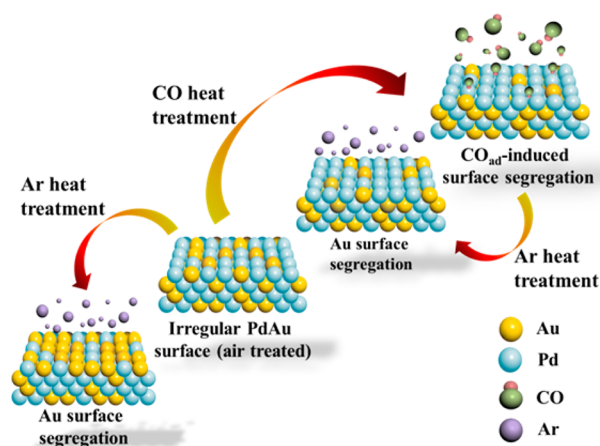


Figure 1. Scheme showing surface states and catalyst activity in selected surfaces following heat treatment.

under a CO atmosphere because the CO adsorption energy is roughly 4 times higher for Pd (−1.32 eV) compared to Au (−0.35 eV),³⁸ whereas Au segregation predominates under an Ar atmosphere because of the lower surface free energy of Au (1.41 J m^{-2}) compared to Pd (2.04 J m^{-2}).^{39,40}

The size of the Pd₃Au/C electrocatalyst nanoparticles was confirmed by TEM. The nanoparticle size distribution was obtained from a sample of ca. 100 particles observed in TEM images (Figure 2). The average size of nanoparticles from TEM was 3.09 ± 0.27 nm, 3.18 ± 0.24 nm, 3.20 ± 0.25 nm, and 3.28 ± 0.21 nm for asp, Ar, CO, and CO–Ar, respectively (Figure S1, see the Supporting Information). Whenever the Pd₃Au/C electrocatalysts were subjected to heat, the nanoparticles increased slightly in size (ca. 0.1 nm) due to the effects of the aggregation and crystalline growth.

The structures, as determined by crystallography, were similar for all of the Pd₃Au/C electrocatalysts (Figure 3), indicating that the samples had a typical face-centered cubic structure. The crystalline sizes of the Pd₃Au/C electrocatalysts were determined as 3.0, 3.1, 3.2, and 3.3 nm for asp, Ar, CO, and CO–Ar, respectively, as determined by the (220) reflection, which corresponds well with the TEM results. The XRD

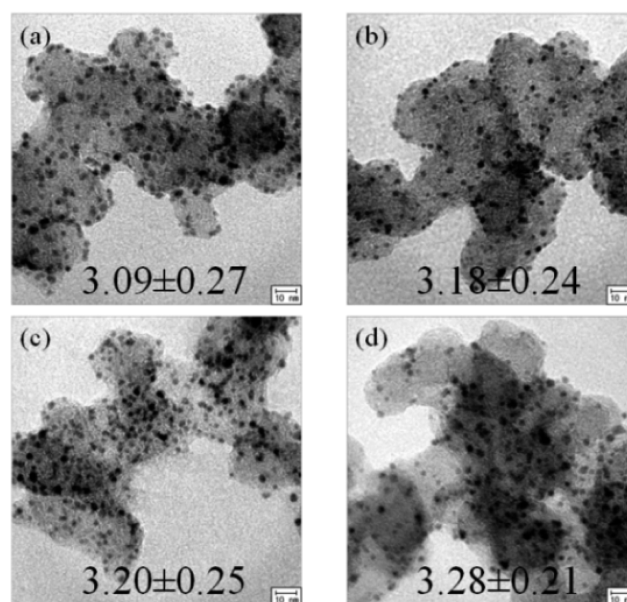


Figure 2. Transmission electron microscopy (TEM) images of 20 wt % Pd₃Au/C electrocatalyst prepared with different heat gas atmospheres: (a) asp, (air) (b) Ar, (c) CO, (d) CO–Ar.

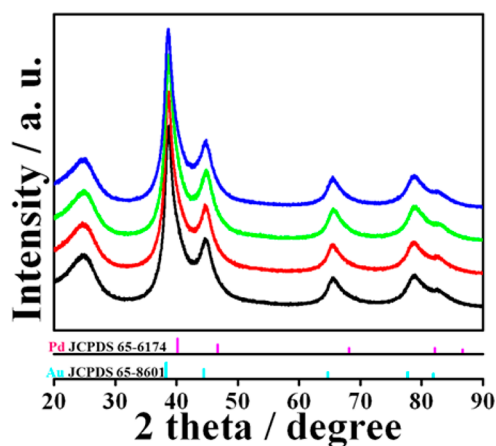


Figure 3. X-ray diffraction of asp (black), Ar (red), CO (green), and CO–Ar (blue).

position of the (220) reflection was located at 65.42° , 65.50° , 65.46° , and 65.58° for asp, Ar, CO, and CO–Ar, respectively. The (220) peak positions of Pd₃Au catalysts were found to be shifted to lower angles compared to pure Pd (68.17° , JCPDS 65–6174). The shifting of peaks to a low angle was demonstrated with the formation of the Pd₃Au alloy.

The electronic structure of each Pd₃Au catalyst was analyzed by XPS (Figure 4). The Pd 3d (335.8 eV) and Au 4f (84.0 eV) binding energies of the Pd₃Au alloy catalyst were determined to be lower in comparison with commercial Pd/C (336.9 eV) and Au/C (84.4 eV) (Figure S2, Table S1); the shift to lower binding energies in Pd/Au alloys is consistent with previous reports.⁴¹ Experimentally, the bulk Pd composition of the Pd₃Au catalysts was determined as 72.1%, 72.4%, 73.3%, and 75.4% for Ar, asp, CO–Ar, and CO, respectively. The Au segregation on the surface of the sample prepared in asp was expected due to the low surface free energy^{42–45} and the small driving force.^{46,47} Furthermore, the intensity ratio of XPS was indicative of bulk catalyst composition due to the mean free

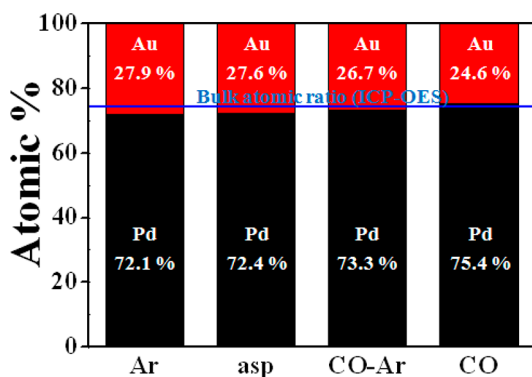


Figure 4. Area ratio between Pd and Au from X-ray photoelectron spectroscopy spectra.

path (>15 Å) with a high kinetic energy (>1000 eV).⁴⁸ The catalyst surface composition was therefore deduced from XPS measured at the surface as well as the core levels. The prepared Pd₃Au/C electrocatalysts were measured with XAS spectra of Pd K-edge. As shown in Figure S3, similar electronic states were observed between Pd from samples. As mentioned above, in light of the XPS results, the limit of X-ray transmission was reached from surface to core level. X-ray species analysis was not measured to surface composition but to bulk scale. Thus, we investigated the surface composition on Pd₃Au catalysts using electrochemical methods.

3.2. Electrochemical Characterizations. Figure 5 shows the results of the CV studies and CO_{ad} oxidation performance for the heat- Pd₃Au catalysts. The electrochemical active surface areas (ESA_{Au} and ESA_{Pd}) were calculated for the Au-oxide

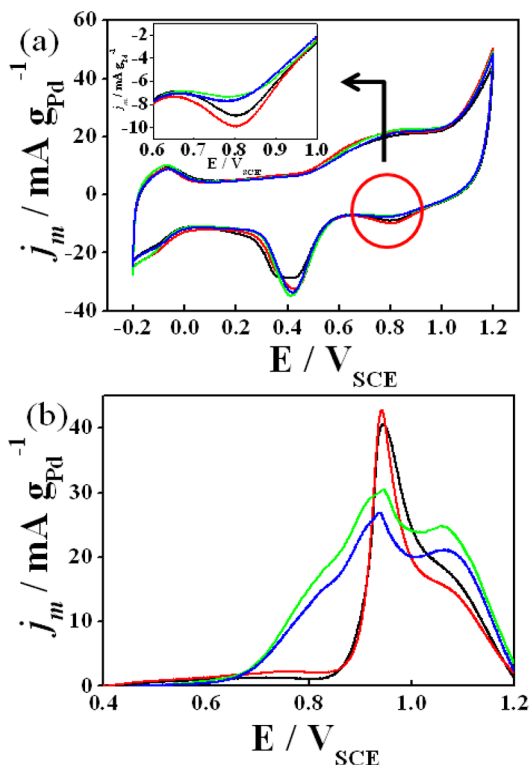


Figure 5. Electrochemical measurements in 0.1 M HClO₄: (a) cyclic voltammograms for electrochemical surface area (ESA_{Au}), and (inset) expansion of ESA_{Au} part, (b) CO_{ad} oxidation curves for ESA_{Pd}: asp (black), Ar (red), CO (green), and CO-Ar (blue).

reduction area and the Pd-CO_{ad} oxidation area. The value of ESA_{Au} was measured as 36.4, 29.8, 24.7, and 23.1 m² g_{Au}⁻¹ for the Ar, asp, CO-Ar, and CO samples, respectively.

The surface composition of Pd was 60.2%, 67.2%, 76.9%, and 80.6% for Ar, asp, CO-Ar, and CO, respectively, using charge values of Au-oxide and CO_{ad} oxidation (ESA_{Pd}/(ESA_{Pd} + ESA_{Au}) in Pd₃Au catalysts), as shown in Figure 6. The CO

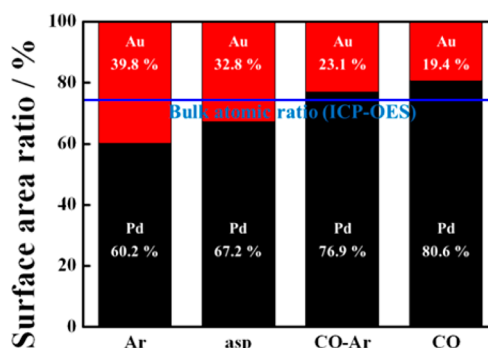


Figure 6. Surface area ratio from ESA of Pd and Au.

sample indicated a ca. 13% increasing of Pd in the Pd-Au ESA ratio as compared to the asp sample. In addition, according to the surface structure of nanoparticles, CO_{ad} oxidation curves were experimentally measured in different shapes depending on the phase, as suggested by Solla-Gullòn et al.⁴⁹ The CO-treated and non-CO-treated samples were observed to produce two distinct curves in their CO_{ad} oxidation peak due to CO coverage on crystallographic phases and the decreased adsorption strength of CO on Pd.^{15,50} The first of peaks of CO and CO-Ar-treated samples are observed at ca. 0.85 V_{SCE}. The observed peak was characteristic of the (100) phase.⁵⁰ The peaks around 0.94 V_{SCE} were deemed to be a combination of low coordination number sites and (111) phases.^{20,49,51} The peaks at 1.04 V_{SCE}, in case of Pt, are attributed to CO_{ad} oxidation on nanoparticle edges, which is predominant in smaller particles.⁵² These results were clear experimental evidence that the nanoparticle surface was Pd enriched and structural modification of surfaces through CO-induced surface segregation was indeed possible.

As shown in Figure 7, the electrocatalytic activities of Pd₃Au nanoparticles were studied by CV in 0.1 M HClO₄ + 0.1 M HCOOH solution. In formic acid oxidation, the asp and Ar

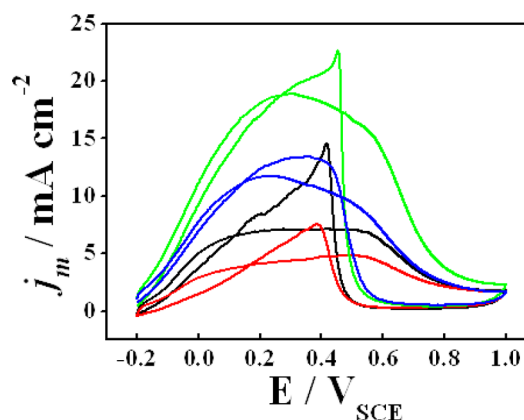


Figure 7. Formic acid oxidation curves of 0.1 M HCOOH in 0.1 M HClO₄: asp (black), Ar (red), CO (green), and CO-Ar (blue).

samples showed the most positive maximum oxidation peaks at 0.49 V_{SCE} . The preceding CO_{ad} oxidation measurement of the asp and Ar samples showed CO stripping peaks at 0.94 V_{SCE} . Therefore, the formic acid oxidation on the Pd surface was mostly indicative of occurring via a direct pathway. The difference arises due to the slow formation of intermediate CO .⁵³ The current density $j_{@0.2V}$ values at 0.2 V_{SCE} of formic acid oxidation on catalysts were 6.93, 4.12, 11.67, and 18.11 $mA\ cm^{-2}$ for asp, Ar, CO–Ar, and CO, respectively. As discussed above, the rate of formic acid oxidation depends on the surface structure: Pd (110) < Pd (111) < Pd (100).¹⁷

As shown in the red of Figure S4, PdOH and Pd₂O are formed on the Pd surface of CO-treated samples at 0.8 V_{SCE} , but the onset of the formic acid oxidation potential (Figure 7) is at a more negative value of $-0.1\ V_{SCE}$. The rapid drop in current of formic acid oxidation was observed at 0.6 V_{SCE} , becoming close to zero at 0.8 V_{SCE} ; the oxidation of formic acid on the Pd nanoparticle surface was inhibited by oxygen donors on the surface. In addition, the dependence of an increase in formic acid oxidation on surface structure modification was proven by the CO-induced surface segregation.

The mass activity ($j_{@0.2V}$ values/Pd loading amount 34.79 $\mu g\ cm^{-2}$ of Pd₃Au catalyst on a GC rotating disk electrode) was 118.42, 199.20, 335.44, and 520.55 $A\ g^{-1}$ for Ar, asp, CO–Ar, and CO, respectively which is denoted by $j_{@0.2V, mass}$ in Figure 8.

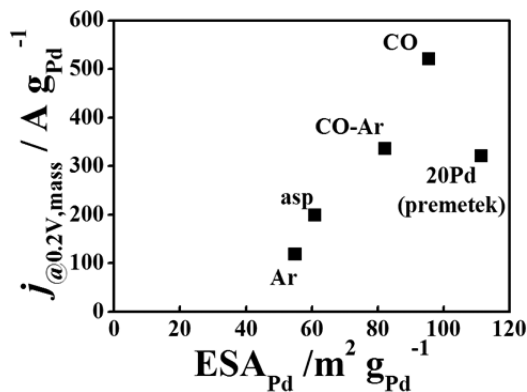


Figure 8. Relationship between ESA_{Pd} and mass activity of Pd₃Au/C electrocatalysts.

The CO sample showed an excellent 2.61-fold increase compared to the asp sample. Through the CO_{ad} oxidation measurement, the ESA_{Pd} was increased about 1.57-fold as compared with the sample. The mass activity of the CO-treated sample was largely enhanced in comparison to the increase in ESA_{Pd} , demonstrating that the fitting (red) was from the origin to CO–Ar sample only (Figure S5).

The specific activity ($j_{@0.2V, mass}$ values/ ESA_{Pd} calculated from CO_{ad} oxidation) was 0.21, 0.33, 0.41, and 0.55 $mA\ cm_{Pd}^{-2}$ for Ar, asp, CO–Ar, and CO, respectively, which is denoted by $j_{@0.2V, area}$ in Figure 9. The specific activity of the CO sample was 1.67 times larger than the asp sample; moving from the Ar to the CO–Ar, the samples saw a gradual increase, before a large increase in activity with the CO sample. Through CO heat treatment, the CO and CO–Ar samples were expected to rearrange their structure in surface reactions. In particular, the CO sample shows a good performance for formic acid oxidation, better than solely through an increase in ESA_{Pd} . The improved performance is caused by the exchange of Au at the surface with Pd in the sublayer; resulting in a state of Pd

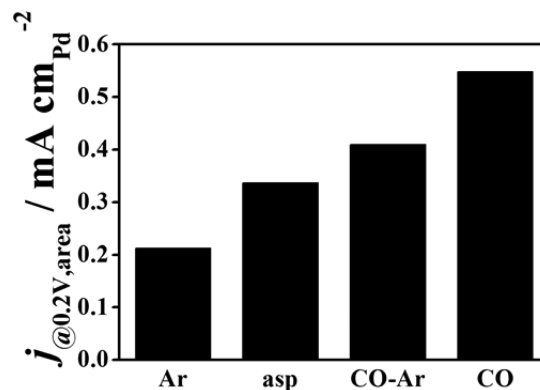


Figure 9. Specific activity ($j_{@0.2V, mass}/ESA_{Pd}$) of Pd₃Au/C electrocatalysts.

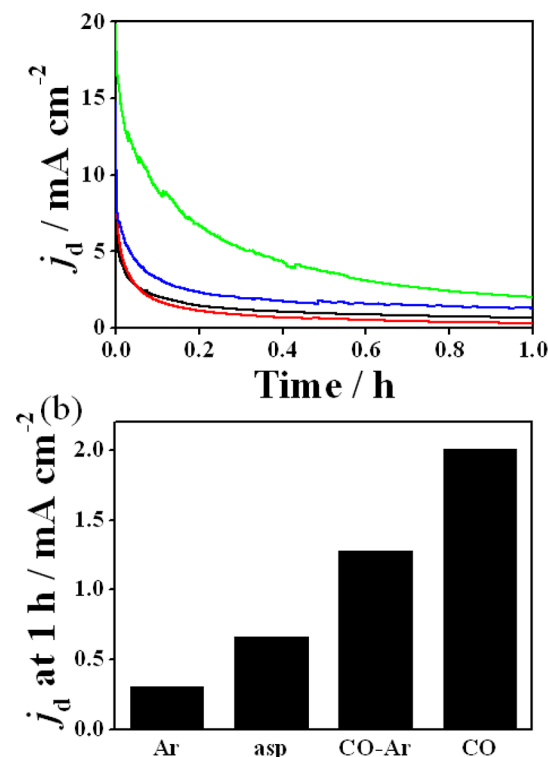


Figure 10. (a) Chronoamperometric curves of 0.1 M HCOOH in 0.1 M HClO₄: asp (black), Ar (red), CO (green), and CO–Ar (blue), (b) j_d at 1 h from chronoamperometry measurements.

enrichment at the surface; the exchange between surface and sublayer occurred simultaneously with the formation of new phases such as (100) phases due to CO-induced surface segregation.

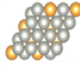
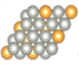
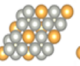
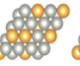
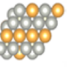
Electrocatalytic stable performance studies of the Pd₃Au nanoparticles were carried out by using CA methods at 0.1 V_{SCE} for 1 h in 0.1 M HClO₄ + 0.1 M HCOOH solution, as shown in Figure 10. The rapid decrease in initial measurement was observed in all samples due to intermediate poisoning species.⁵ The CO-treated sample, however, decreased more slowly than the others. For the interaction between surface Pd and Au in the sublayers, the surface Pd metal gained d-electrons from the Au sublayer, which responded by weakening the adsorptive strength of the reaction intermediate in formic acid oxidation.⁵⁴ The current density values of CA after 1 h were 0.30, 0.66, 1.28, and 2.01 for Ar, asp, CO–Ar, and CO, respectively. The CO-

treated sample was determined to have a higher electrocatalytic CA test than the other samples after 1 h. The electrochemical measurement values are summarized in Table S2.

The changes to surface structure and Pd concentration could be compared to the performance between samples generated by CO-induced surface segregation and non-CO-treated samples. The enhanced stability and formic acid oxidation activity are demonstrated to not only depend on ligand effects (including the influence of electronic, strain, and bonding factors)^{55,56} but also the ensemble effect that describes the synergistic effect in different surface composition arrangements.⁵⁷ This study suggests that the carbon-supported alloy nanoparticle catalysts could be obtained to enhance both the oxidation of formic acid and stable performance without changing the metal composition through CO-induced surface segregation.

3.3. DFT Calculations. To better understand the effect of CO-induced surface segregations on the oxidation of formic acid, DFT calculations were performed. For such purposes, we calculated the reaction energetics (ΔE_{HCOO}) for the rate-determining step (RDS) ($\text{HCOO} \rightarrow \text{CO}_2(\text{g}) + \text{H}$)⁵⁸ of formic acid oxidation by varying the surface composition of Pd in Table 1. We modeled the surface segregation by exchanging Au atoms

Table 1. Calculated Reaction Energetic for $\text{HCOO} \rightarrow \text{CO}_2(\text{g}) + \text{H}$ as a Function of Surface Pd Composition

Surface Pd (%)	88	81	75	69	63
Surface layer	$\text{Pd}_{14}\text{Au}_2$	$\text{Pd}_{13}\text{Au}_3$	$\text{Pd}_{12}\text{Au}_4$	$\text{Pd}_{11}\text{Au}_5$	$\text{Pd}_{10}\text{Au}_6$
2 nd layer	$\text{Pd}_{10}\text{Au}_6$	$\text{Pd}_{11}\text{Au}_5$	$\text{Pd}_{12}\text{Au}_4$	$\text{Pd}_{13}\text{Au}_3$	$\text{Pd}_{14}\text{Au}_2$
3 rd layer					
4 th layer			$\text{Pd}_{12}\text{Au}_4$		
5 th layer					
Top view					
$\text{HCOO} \rightarrow \text{CO}_2 + \text{H}$ RDS decomposition energy (eV)	-0.70	-0.68	-0.66	-0.36	-0.41

in the top surface layer of an ordered slab of Pd_3Au alloy with Pd atoms in the second surface layer. We found that the reaction energetics strongly depended on the Pd surface composition. In particular, the alloy surface with a relatively high Pd content (>75%) shows a higher exothermicity for $\text{HCOO} \rightarrow \text{CO}_2(\text{g}) + \text{H}$ [$\Delta E_{\text{HCOO}} = -0.70$ eV (for a surface of 88% Pd), -0.68 eV (81%), -0.66 eV (75%)] than a case with relatively low Pd content [$\Delta E_{\text{HCOO}} = -0.36$ eV (69%), -0.41 eV (63%)], implying that the increase of surface Pd content by CO treatment makes the formic acid oxidation more thermodynamically favorable. This activity difference may be related to the availability of the 3-fold hollow sites (S_{HW}) associated with one Au and two Pd atoms [indicated by $S_{\text{HW}}(2\text{Pd}_1\text{Au})$ in Figure 11] whose population increases by decreasing the Pd content on the alloy surface. Our DFT calculations predict that the binding strength of H on the $S_{\text{HW}}(2\text{Pd}_1\text{Au})$ site substantially decreases by 0.26 eV, compared to the hollow site associated with three Pd atoms [indicated by $S_{\text{HW}}(3\text{Pd})$ in Figure 11]. Note that the 3-fold adsorption mode for H is the most favorable, and thus the H radical on the $S_{\text{HW}}(2\text{Pd}_1\text{Au})$ site is associated with one relatively inert Au atom. Conversely, the binding strength of HCOO on the $S_{\text{HW}}(2\text{Pd}_1\text{Au})$ site is calculated to be similar to the $S_{\text{HW}}(3\text{Pd})$ case. Here, HCOO follows the 2-fold adsorption mode, and thus the Au atom on the $S_{\text{HW}}(2\text{Pd}_1\text{Au})$ site is not involved in

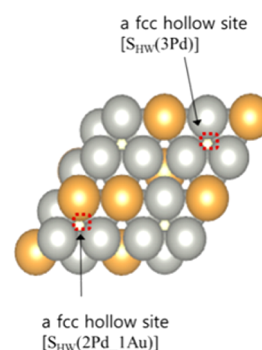


Figure 11. Two different face-centered cubic hollow sites (a) associated with one Au and two Pd atoms; (b) with three Pd atoms. Yellow and gray balls represent the Au and Pd atom, respectively.

HCOO adsorption. Correspondingly, for the $S_{\text{HW}}(2\text{Pd}_1\text{Au})$ case, the potential energy level of the products in the $\text{HCOO} \rightarrow \text{CO}_2(\text{g}) + \text{H}$ reaction substantially increases, whereas for the $S_{\text{HW}}(3\text{Pd})$ case, the potential energy level of the reactant side does not change. As a result, the reaction energetics for the $\text{HCOO} \rightarrow \text{CO}_2(\text{g}) + \text{H}$ on the $S_{\text{HW}}(2\text{Pd}_1\text{Au})$ site are less exothermic than the $S_{\text{HW}}(3\text{Pd})$ case.

4. CONCLUSION

A surface segregation of Pd in $\text{Pd}_3\text{Au}/\text{C}$ nanoparticles was successfully achieved changing the structure and composition of the surface. Formic acid oxidation by the CO-treated sample was improved (from 6.93 to 18.11 mA cm^{-2}), in addition to the stability (from 0.66 to 2.01 mA cm^{-2}), as well as increasing the ESA_{Pd} (from 61.08 to 95.68 $\text{m}^2 \text{g}_{\text{Pd}}^{-1}$) and the specific activity (from 0.33 to 0.55 $\text{mA cm}_{\text{Pd}}^{-2}$) in comparison to the asp sample. DFT calculations also showed that the RDS of formic acid oxidation depends on the relative Pd contents of the surfaces (>75%). Therefore, the improved formic acid oxidation of the CO-treated sample which exhibited greatly improved stable performance than the other samples due to Pd enrichment of the surface was attributed to depend on an efficient, direct pathway, as well as the exchange between surface Pd and sublayer Au due to the difference in CO binding energy. The CO-induced surface segregation simultaneously influences not only the Pd enrichment of the surface but also changes to the surface structure. We suggest that the CO-induced surface segregation method can be applied to accomplish greatly enhanced surface performance by changing surfaces with a lower Pd content to an optimum structure and surface composition. It may also be possible to manipulate other metal catalyst surfaces in similar fashion. The results obtained in this study are a highly promising development in the continued quest for step changes in the improvement of fuel cell technology, which are central to society's need to develop viable renewable energy technologies.

■ ASSOCIATED CONTENT

Supporting Information

Particle size distribution histogram of $\text{Pd}_3\text{Au}/\text{C}$ electrocatalysts, XPS spectra of Pd 3d and Au 4f, normalized XAS spectra of Pd K-edge, CO_{ad} oxidation, relationship between ESA_{Pd} and mass activity, and XPS spectra measurement value in this study. This material is available free of charge via the Internet at <http://pubs.acs.org>.

AUTHOR INFORMATION

Corresponding Authors

*E-mail: hjjang@kist.re.kr. Fax: +82-958-5199. Tel.: +82-958-5287.

*E-mail: ysj@kist.re.kr. Fax: +82-958-5199. Tel.: +82-958-5260.

Notes

The authors declare no competing financial interest.

ACKNOWLEDGMENTS

This work was supported by the Global Frontier R&D Program on Center for Multiscale Energy System funded by NRF under MSIP, Korea (no. 2012M3A6A7054283) and supported by NRF grant funded by MSIP, Korea (no. 2014R1A2A2A04003865). This work was also supported by KRCRC grant funded by MSIP, Korea (no. 2013M1A8A1038315) and by the New & Renewable Energy Core Technology Program of KETEP grant funded by MOTIE, Korea (no. 20133030011320).

REFERENCES

- (1) Zhou, W.; Lee, J. Y. *J. Phys. Chem. C* **2008**, *112*, 3789.
- (2) Larsen, R.; Ha, S.; Zakzeski, J.; Masel, R. I. *J. Power Sources* **2006**, *157*, 78.
- (3) Larsen, R.; Zakzeski, J.; Masel, R. I. *Electrochem. Solid-State Lett.* **2005**, *8*, A291.
- (4) Liu, Y.; Wang, L.; Wang, G.; Deng, C.; Wu, B.; Gao, Y. *J. Phys. Chem. C* **2010**, *114*, 21417.
- (5) Qin, Y. H.; Jiang, Y.; Niu, D. F.; Zhang, X. S.; Zhang, X. S.; Niu, L.; Yuan, W. K. *J. Power Sources* **2012**, *215*, 130.
- (6) Wang, X.; Hu, J.-M.; Hsing, I.-M. *J. Electroanal. Chem.* **2004**, *562*, 73.
- (7) Feng, Y.-Y.; Zhang, G.-R.; Xu, B.-Q. *RSC Adv.* **2013**, *3*, 1748.
- (8) Osawa, M.; Komatsu, K. I.; Samjeské, G.; Uchida, T.; Ikeshoji, T.; Cuesta, A.; Gutiérrez, C. *Angew. Chem., Int. Ed.* **2011**, *50*, 1159.
- (9) Rice, C.; Ha, S.; Masel, R. I.; Wieckowski, A. *J. Power Sources* **2003**, *115*, 229.
- (10) Nishimura, K.; Kunimatsu, K.; Machida, K. I.; Enyo, M. *J. Electroanal. Chem.* **1989**, *260*, 181.
- (11) Cuesta, A.; Escudero, M.; Lanova, B.; Baltruschat, H. *Langmuir* **2009**, *25*, 6500.
- (12) Huang, Y.; Zhou, X.; Yin, M.; Liu, C.; Xing, W. *Chem. Mater.* **2010**, *22*, 5122.
- (13) Park, I. S.; Lee, K. S.; Yoo, S. J.; Cho, Y. H.; Sung, Y. E. *Electrochim. Acta* **2010**, *55*, 4339.
- (14) Montes de Oca, M. G.; Plana, D.; Celorrio, V.; Lazaro, M. J.; Fermin, D. J. *J. Phys. Chem. C* **2011**, *116*, 692.
- (15) Zhang, G.; Wang, Y.; Wang, X.; Chen, Y.; Zhou, Y.; Tang, Y.; Lu, L.; Bao, J.; Lu, T. *Appl. Catal., B* **2011**, *102*, 614.
- (16) Chen, M.; Kumar, D.; Yi, C. W.; Goodman, D. W. *Science* **2005**, *310*, 291.
- (17) Hoshi, N.; Kida, K.; Nakamura, M.; Nakada, M.; Osada, K. *J. Phys. Chem. B* **2006**, *110*, 12480.
- (18) Christensen, A.; Ruban, A. V.; Stoltze, P.; Jacobsen, K. W.; Skriver, H. L.; Nørskov, J. K.; Besenbacher, F. *Phys. Rev. B* **1997**, *56*, 5822.
- (19) Jeon, T. Y.; Lee, K. S.; Yoo, S. J.; Cho, Y. H.; Kang, S. H.; Sung, Y. E. *Langmuir* **2010**, *26*, 9123.
- (20) Chung, D. Y.; Chung, Y. H.; Jung, N.; Choi, K. H.; Sung, Y. E. *Phys. Chem. Chem. Phys.* **2013**, *15*, 13658.
- (21) Jacobsen, C. J. H.; Dahl, S.; Clausen, B. S.; Logadottir, A.; Nørskov, J. K. *J. Am. Chem. Soc.* **2001**, *123*, 8404.
- (22) Besenbacher, F.; Chorkendorff, I.; Clausen, B. S.; Hammer, B.; Molenbroek, A. M.; Nørskov, J. K.; Stensgaard, I. *Science* **1998**, *279*, 1913.
- (23) Studt, F.; Abild-Pedersen, F.; Bligaard, T.; Sørensen, R. Z.; Christensen, C. H.; Nørskov, J. K. *Science* **2008**, *320*, 1320.
- (24) Menning, C. A.; Hwu, H. H.; Chen, J. G. *J. Phys. Chem. B* **2006**, *110*, 15471.
- (25) Nerlov, J.; Chorkendorff, I. *J. Catal.* **1999**, *181*, 271.
- (26) Christoffersen, E.; Stoltze, P.; Nørskov, J. K. *Surf. Sci.* **2002**, *505*, 200.
- (27) Nerlov, J.; Sckerl, S.; Wambach, J.; Chorkendorff, I. *Appl. Catal., A* **2000**, *191*, 97.
- (28) Bagot, P. A. J.; Cerezo, A.; Smith, G. D. W.; de Mocarme, T. V.; Godfrey, T. *J. Surf. Interface Anal.* **2007**, *39*, 172.
- (29) Lee, K. S.; Park, H. Y.; Ham, H. C.; Yoo, S. J.; Kim, H. J.; Cho, E. A.; Manthiram, A.; Jang, J. H. *J. Phys. Chem. C* **2013**, *117*, 9164.
- (30) Park, H. Y.; Jeon, T. Y.; Jang, J. H.; Yoo, S. J.; Choi, K. H.; Jung, N.; Chung, Y. H.; Ahn, M.; Cho, Y. H.; Lee, K. S.; Sung, Y. E. *Appl. Catal., B* **2013**, *129*, 375.
- (31) Greeley, J.; Mavrikakis, M. *Catal. Today* **2006**, *111*, 52.
- (32) Friedrich, K. A.; Marmann, A.; Stimming, U.; UnKauf, W.; Vogel, R. *Fresenius' J. Anal. Chem.* **1997**, *358*, 163.
- (33) Friedrich, K. A.; Marmann, A.; Stimming, U.; UnKauf, W. *Colloids Surf., A* **1998**, *134*, 193.
- (34) Moore, A.; Celorrio, V.; Montes de Oca, M.; Plana, D.; Hongthani, W.; Lazaro, M. J.; Fermin, D. J. *Chem. Commun.* **2011**, *47*, 7656.
- (35) Perdew, J. P.; Wang, Y. *Phys. Rev. B: Condens. Matter Mater. Phys.* **1992**, *45*, 13244.
- (36) Kresse, G.; Furthmüller, J. *VASP the Guide*; Vienna University of Technology: Vienna, Austria, 2001.
- (37) Blöchl, P. E. *Phys. Rev. B: Condens. Matter Mater. Phys.* **1994**, *50*, 17953.
- (38) Zhang, J.; Jin, H.; Sullivan, M. B.; Lim, F. C. H.; Wu, P. *Phys. Chem. Chem. Phys.* **2009**, *11*, 1441.
- (39) Kumikov, V. K.; Khokonov, Kh. B. *J. Appl. Phys.* **1983**, *54*, 1346.
- (40) Mezey, L. Z.; Giber, J. *Appl. Phys. A: Solids Surf.* **1984**, *35*, 87.
- (41) Nascente, P. A. P.; de Castro, S. G. C.; Landers, R.; Kleiman, G. *Phys. Rev. B* **1991**, *43*, 4659.
- (42) Wei, T.; Wang, J.; Goodman, D. W. *J. Phys. Chem. C* **2007**, *111*, 8781.
- (43) Greeley, J.; Jaramillo, T. F.; Bonde, J.; Chorkendorff, I.; Nørskov, J. K. *Nat. Mater.* **2006**, *5*, 909.
- (44) Ruban, A. V.; Hammer, B.; Stoltze, P.; Skriver, H. L.; Nørskov, J. K. *J. Mol. Catal. A: Chem.* **1997**, *115*, 421.
- (45) Ruban, A. V.; Skriver, H. L.; Nørskov, J. K. *Phys. Rev. B* **1999**, *59*, 15990.
- (46) Yuan, D.; Gong, X.; Wu, R. *Phys. Rev. B* **2007**, *75*, 085428.
- (47) Kibler, L. A. *Electrochim. Acta* **2008**, *53*, 6824.
- (48) Tao, F.; Grass, M. E.; Zhang, Y.; Butcher, D. R.; Renzas, J. R.; Liu, Z.; Chung, J. Y.; Mun, B. S.; Salmeron, M.; Somorjai, G. A. *Science* **2008**, *322*, 932.
- (49) Solla-Gullón, J.; Vidal-Iglesias, F. J.; Herrero, E.; Feliu, J. M.; Aldaz, A. *Electrochem. Commun.* **2006**, *8*, 189.
- (50) Hara, M.; Linke, U.; Wandlowski, T. *Electrochim. Acta* **2007**, *52*, 5733.
- (51) Brimaud, S.; Pronier, S.; Coutanceau, C.; Léger, J. M. *Electrochem. Commun.* **2008**, *10*, 1703.
- (52) Guerin, S.; Hayden, B. E.; Lee, C. E.; Mormiche, C.; Owen, J. R.; Russell, A. E.; Theobald, B.; Thompsett, D. *J. Comb. Chem.* **2004**, *6*, 149.
- (53) Lu, G. Q.; Crown, A.; Wieckowski, A. *J. Phys. Chem. B* **1999**, *103*, 9700.
- (54) Zhou, W.; Lee, J. Y. *Electrochem. Commun.* **2007**, *9*, 1725.
- (55) Kitchin, J. R.; Nørskov, J. K.; Barteau, M. A.; Chen, J. G. *Phys. Rev. Lett.* **2004**, *93*, 156801.
- (56) Rodriguez, J. A.; Goodman, D. W. *Science* **1992**, *257*, 897.
- (57) Maroun, F.; Ozanam, F.; Magnussen, O. M.; Behm, R. J. *Science* **2001**, *293*, 1811.
- (58) Ojeda, M.; Iglesia, E. *Angew. Chem., Int. Ed.* **2009**, *48*, 4800.